Live Cell Interferometry Reveals Cellular Dynamism During Force Propagation

Jason Reed,[†,⊥] Joshua J. Troke,[‡] Joanna Schmit,[§] Sen Han,[§] Michael A. Teitell,[‡,⊥,∥,*] and James K. Gimzewski[†,⊥,*]

[†]Department of Chemistry and Biochemistry, University of California, Los Angeles, 607 Charles Young Drive East, Los Angeles, California, 90095, [‡]Department of Pathology and Laboratory Medicine, and [∥]Jonsson Comprehensive Cancer Center, Institute for Stem Cell Biology and Medicine (ISCBM), and Molecular Biology Institute, David Geffen School of Medicine at University of California, Los Angeles, 10833 Le Conte Avenue, Los Angeles, California 90095-1732, [§]Veeco Instruments, Inc., 2650 East Elvira Road, Tucson, Arizona 85711, [⊥]California NanoSystems Institute (CNSI), 570 Westwood Plaza, Los Angeles, California 90095

ABSTRACT Cancer and many other diseases are characterized by changes in cell morphology, motion, and mechanical rigidity. However, in live cell cytology, stimulus-induced morphologic changes typically take 10–30 min to detect. Here, we employ live-cell interferometry (LCI) to visualize the rapid response of a whole cell to mechanical stimulation, on a time scale of seconds, and we detect cytoskeletal remodeling behavior within 200 s. This behavior involved small, rapid changes in cell content and miniscule changes in shape; it would be difficult to detect with conventional or phase contrast microscopy alone and is beyond the dynamic capability of AFM. We demonstrate that LCI provides a rapid, quantitative reconstruction of the cell body with no labeling. This is an advantage over traditional microscopy and flow cytometry, which require cell surface tagging and/or destructive cell fixation for labeling

KEYWORDS: interferometry · cytoskeleton remodeling · live-cell imaging

Mammalian cells exhibit continuous regional motion and shape changes controlled by a dynamic cytoskeleton. The movements of a cell are orchestrated by a dynamic cytoskeleton that extends from the fluid lipid bilayer and underlying Actin cortex to deep within a cell. The mechanical scaffold of each cell is composed of relatively stiff components including Actin microfilaments, intermediate filaments, microtubules, and a myriad of cross-linking, motor, and regulatory proteins that maintain structure and control dynamism. Numerous studies link these cytoskeletal structures to biochemical signal transduction pathways to regulate cellular processes including adhesion, motility, gene expression, and differentiation.[1−7] A key challenge that remains is connecting specific structures and signaling to the changing biophysical properties of the cell and *vice-versa*. A critical issue in probe-based measurements of cell mechanics, such as AFM and optical/magnetic tweezers, is the speed and degree to which a mechanical force exerted by a probe propagates across the cell body.[8] This is seldom documented because observing deformation of the entire cell body with required speed and accuracy (∼1% local deformation) is experimentally complex, for a variety of reasons. For example, in most cases AFM cannot accurately image the membrane of an entire mammalian cell at the rate of 1−2 Hz, because of the softness of the cell membrane. Bead-based approaches, such as magnetic and optical traps, track the motion of the bead itself and not the surrounding cellular material which is unlabeled. Labels can be introduced but this adds considerable complexity. With phase contrast methods organelles themselves can serve as displacement probes, but they are not uniformly distributed. This is a major constraint when investigating dynamic structures not containing organelles, such as filopodia.

To address these problems, we have developed a novel imaging technique, called live-cell interferometry (LCI), to directly assess the propagation of strain throughout a single cell in response to locally applied force. By measuring changes in optical path length distribution across many points within the cell simultaneously, we could determine the corresponding redistribution of cellular constituents, and thus could quantify responses of the cell body distal to the point of applied force in real time and without labeling. Our imaging system (Figure 1) consists of an optical microscope with a Michelson interference objective, a fluid-filled live-cell observation chamber with a reflective floor, and a matched reference chamber containing only fluid. It operates as follows: The illumination wavefront incident on the observation chamber travels through the transparent fluid (culture media) and the transparent cell body and is returned to the interferometer by the reflec-

Ⓦ This paper contains enhanced objects available on the Internet at http://pubs.acs.org/journals/ancac3.

*Address correspondence to gim@chem.ucla.edu, mteitell@ucla.edu.

Received for review October 16, 2007 and accepted April 09, 2008.

10.1021/nn700303f CCC: $40.75

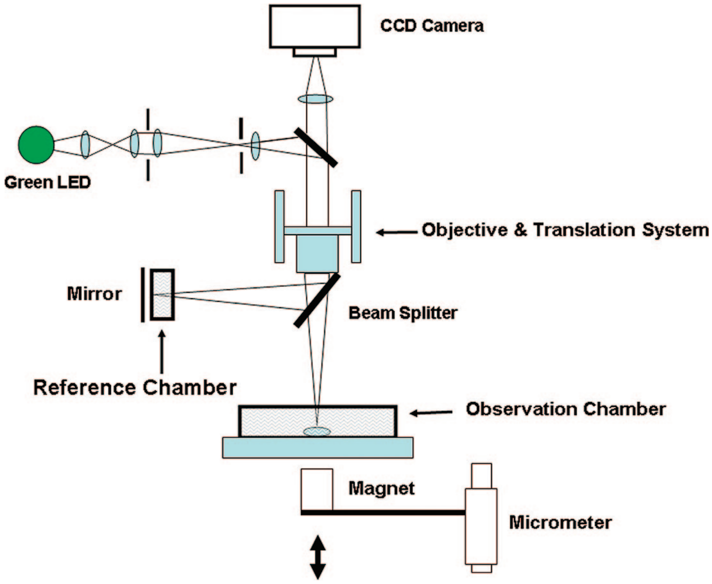

Figure 1. The interferometric microscope uses a 20× long working-distance objective, in combination with a Michelson interferometer containing an adjustable mirror in the reference arm. A fluid compensation chamber is positioned in the interferometer's reference arm to permit measurements inside the media-filled cell chamber. Dimensions of the compensation chamber were adjusted to closely match the optical path length between the test and reference arms. Live cells were imaged in a perfusion chamber maintained at 5% CO_2 and 37 °C. A cylindrical rare-earth magnet mounted on a micrometer is positioned below the perfusion chamber. The magnitude of the magnetic force applied to the magnetic microspheres inside the cell chamber was adjusted by varying the distance between the magnet pole face and the sample.

tive substrate. The index of refraction of the culture media and the cell body are so close in value that there is very little reflection of the light from the cell–fluid interface. However, the difference in the index of refraction of the fluid and cell is sufficiently large for the detection of changes in optical path length introduced by the cell as the light travels through it and is reflected back from the substrate. The optical path length is the geometrical path the wavefront travels times the index of refraction distribution $n(z)$ of the media at a given point. Because the light reflects from the substrate and returns to the objective, it travels twice the same geometric distance z, the sample optical path length can be expressed as

$$2\int n(z)\,\mathrm{d}z \tag{1}$$

While for the light traveling through the reference chamber fluid, having a uniform distribution of index of refraction, the reference optical path length is simply

$$2zn_{\text{fluid}} \tag{2}$$

In the LCI technique, this difference in optical path is recorded as a shift in phase between the sample observation and reference beams.[9] The resulting LCI phase image shows a distribution of the optical path lengths in the field of view of the objective. Obtained in this way the signature of the cell shows that the optical path length is longer through the cell *versus* fluid by about 0–400 nm (Figure 2). This data agrees with the assumption that the index of refraction of the fluid is about 1.33, the index of refraction for the cell body is 1.4–1.5, and the maximum thickness of the cell is about 5–8 μm. Thus, the measured optical path length represents the distribution of cells' thickness and material index of refraction together.

RESULTS AND DISCUSSION

By comparing optical path length images taken at two consecutive time points, we determined very precisely local shifts of material within the cell. This is illustrated in Figure 2. We were able to reliably detect changes in optical path length as small as ~1 nanometer. Since the cell body appears to be

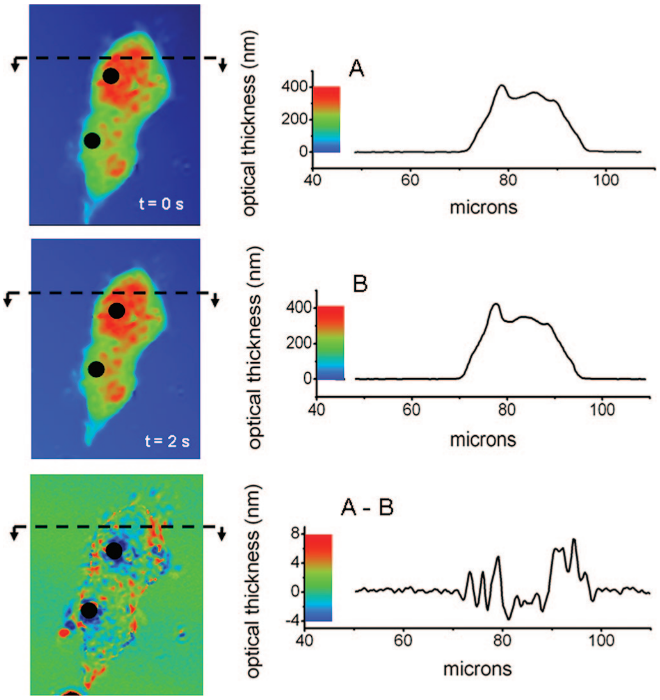

Figure 2. (Top two panels) LCI interferometric images of a live NIH 3T3 fibroblast taken two seconds apart, before and after the application of force by two magnetic microspheres on their surface (indicated by black disks). The optical thickness cross-sections are displayed to the right. (Lower panel) The change in optical thickness between the two images is readily apparent in the differential LCI image, created by subtracting the bottom from the top LCI image. The optical thickness of the cell body ranges from 0 to 400 nm and the change in optical thickness detectable in the differential LCI image ranges from −6 to +8 nm.

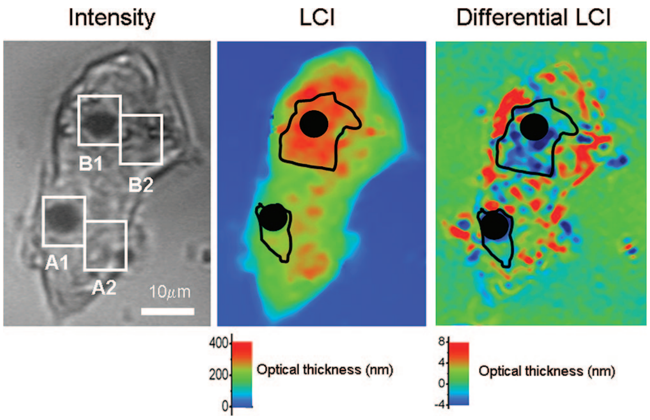

Figure 3. Intensity (left) and LCI interferometric (right) images of a single NIH3T3 cell with two magnetic microspheres on the cell surface. As force was applied to the probes, we tracked the change in optical path length in the regions directly surrounding each probe (A1 and B1), and the adjacent regions (A2 and B2). A 200 pN peak-to-trough 0.05 Hz cyclical force was applied to the microspheres for 200 s.

between 0 and 400 nm in optical thickness, this corresponds to the ability to detect <1% changes in optical path length over large portions of the cell.

We recorded shifts in optical thickness in regions adjacent to magnetic microspheres undergoing cyclical indentations at 0.05 Hz for 200 s or 10 cycles (Figure 3). Two 5 µm diameter microspheres were evaluated simultaneously on an elongated NIH 3T3 fibroblast. The maximum applied force was ~200 pN for each microsphere. The mechanical linkage between the force-driven and undriven regions of the cell was measured as the change in the optical thickness profiles over each indentation cycle. A shift in cell content was not readily apparent in either the intensity image or the LCI image itself but was detected by comparing the difference between two LCI images. This differential LCI image provided a quantitative measure of the redistribution of material in the cell in response to the indenting body for any two time points. A digital movie of a single indentation cycle is attached to Figure 4. In these experiments two features became apparent: first, the strain field due to the indenting sphere extends across the entire cell, in a pattern that suggests displacement of core underlying, rigid structures (Figure 4); and second, the indentation produces an immediate, synchronized, and laterally continuous increase in material at the cell periphery, consistent with pressure-driven flow. Detecting these rapid rearrangements in the local material density would be difficult with noninterference-based optical methods and is beyond the dynamic capability of AFM. Optical waveguides have been used to observe the nanometer-scale deformation of a metallic substrate surface caused by a plant fungus.[10] This method is confined to reflective surfaces however, whereas LCI measures subtle index of refraction changes of a volume of transparent material (the cell body).

We analyzed the time-dependence of the content shift between specific regions of the cell by measuring the change in average optical thickness within four subregions of the cell body (Figure 3 left). The undriven regions responded at the same frequency as the driven regions, but with a temporal delay, as would be expected from a viscoelastic material (Supporting Information, Figure 2). The amplitudes of motion of both the driven and undriven regions increased with time (Figure 5). In the driven region A1 the amplitude peaked at ~100 s and leveled off, while the amplitude of the other region, B1, peaked later (~150 s), and then began to decline. This behavior suggests that the local compliance of the cell changed with time and that this change was distributed heterogeneously within the cell.

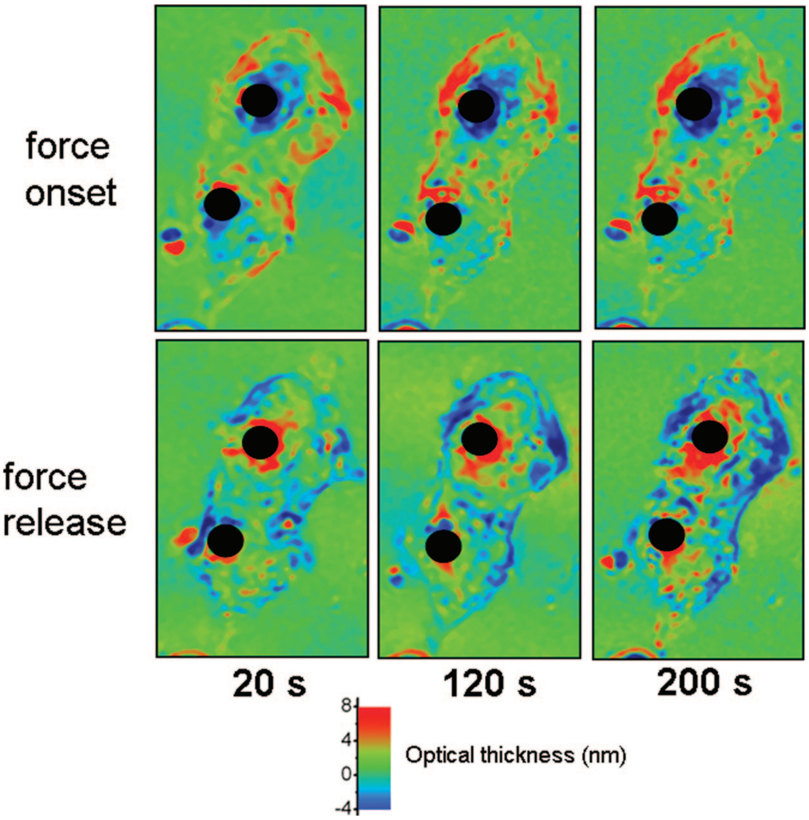

Figure 4. Differential LCI images of three indentation cycles spanning 200 s. The top series of images shows the effect of probe indentation immediately after force is applied and the bottom series shows the corresponding rebound after force is removed. The pattern and magnitude of material redistribution appears to change with time.

Ⓦ **A movie of a single indentation cycle is available.**

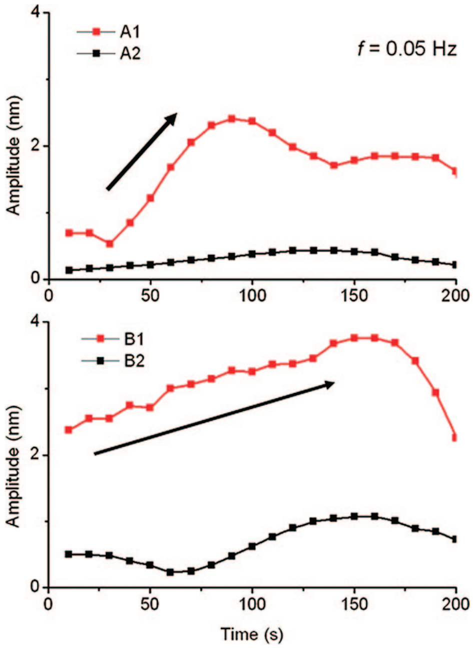

Figure 5. The effect of 0.05 Hz cyclical loading on the adjacent cellular regions is seen as a change in average optical thickness. The cyclic amplitude of the time-varying change optical thickness of regions A1 and A2 evaluated at frequency = 0.05 Hz show the relationship between the driven and undriven portions of the cell body (top). Similar behavior is seen in regions B1 and B2 (bottom). The regions adjacent to the probes show a clear response, indicating that the strain field within the cell body extends several probe diameters laterally. Individual data points are collected at 2 s intervals, for a 0.5 Hz sampling frequency. For clarity, the data have been band-pass filtered with a 0.05 Hz center frequency.

After 200 s of cyclically applied force, there was a noticeable, nontransient redistribution of material within the cell body. The magnitude of this shift was larger than the transient response, with maximum local changes in content of 10−15%, but was still observable only in the differential LCI images (Figure 6). Material accumulated in the center of the cell, preferentially along the "backbone" of the long axis. Lamellepodia also formed at either end of the cell parallel to the long axis. There was an opposing loss of material at the edges of the cell adjacent to the two microspheres, parallel with the short axis of the cell. Notably, the regions with the largest decrease in material over 200 s corresponded to the regions of the cell which saw the most transient change in content during each earlier force cycle. The forced motion was ended at $t = 200$ s and the cell was imaged again at $t = 400$ s. By this time, the pattern of material accumulation within the cell had largely reversed, the lamellepodia parallel to the long axis retracted, and material accumulated adjacent to each microsphere, parallel to the short axis of the cell. This behavior suggests an active remodelling of the cytoskeleton in response to cyclic loading.[2] Local force-induced remodeling is known to begin within tens of seconds following a mechanical stimulus.[11] The edges of the cell retracted and then re-extended at a linear velocity of approximately 180 nm per second, which is consistent with active, actinomyosin-driven motion. The accumulation of material along the cell "backbone" is also consistent with enhanced cytoskeletal contractility, known to occur in some cells following forced stretching or similar mechanical deformations.[11−13]

There was a considerable transient change in content near the cell periphery during each force cycle, the same areas that showed the greatest nontransient shift in material accumulation. Overall, this behavior demonstrates a global coordination and reorientation of the cell structure in response to a local, cyclically applied stress. The mechanisms triggering this content rearrangement could include both phosphatase-integrin complex activation,[2,3,5] and membrane stretch-activated ion channel function.[4,14] The latter have been shown to induce tail retraction in migrating keratocytes and are known to trigger a calcium-dependent signaling cascade that results in the phosphorylation of myosin, leading to retraction of filipodia.[4,14] The synchronized and laterally continuous increase in material at the periphery of the cell in response to indentation seems likely to have disturbed the cell membrane in these areas and suggests that membrane stretch mechanisms need to be considered.[2,15]

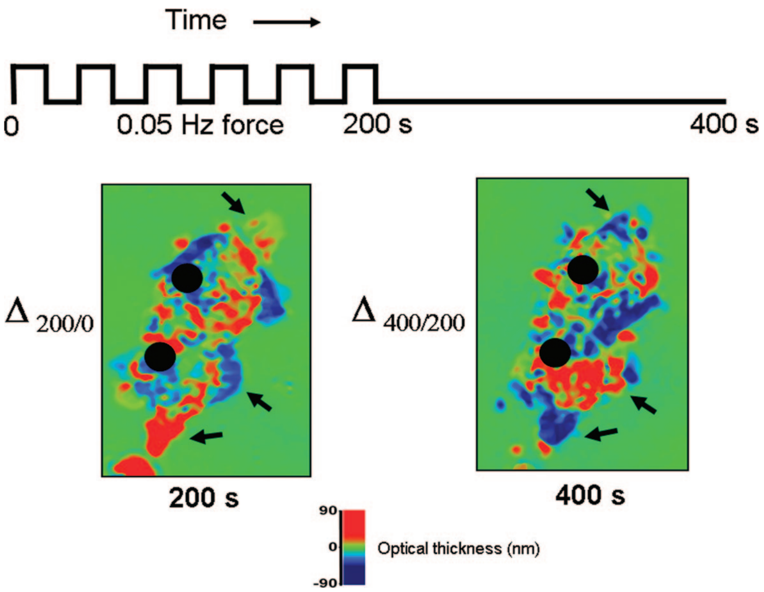

Figure 6. Differential LCI comparison of material distributions after $t = 200$ s of cyclically applied force (Δ 200/0) and at 200 s after cessation of force ($t = 400$ s; Δ 400/200). The positions of the microspheres are indicated by black circles. Arrows denote regions of material redistribution within the cell.

In many magnetic/optical tweezer experiments, and some AFM experiments, the probe is coated with a peptide ligand to promote specific attachment to cell surface receptors. In theory, this allows a direct mechanical link to the cytoskeleton, which could propagate an applied force to other regions of the cell and a vehicle for studying whole cell mechanical dynamics. However, in practice the degree of attachment to the cytoskeleton is seldom confirmed, and conflicting results have been reported regarding the degree of force propagation.[2,16] In some cases experimenters have observed the displacement of organelles or injected particles to infer the strain field, though this produces only a sampling and not a global measurement.[17,18] Various labeling schemes can make this sort of measurement more comprehensive, but often require engineered cell lines or tedious labeling procedures that limit their use. LCI is compatible with these existing approaches, and addresses one of their significant weaknesses by globally capturing the redistribution of cell material in response to force. This spatially and temporally detailed tracking of cell material also may have utility in improving computational models of cell mechanics, which are now largely phenomenological[19–22] and have difficulty assigning specific model parameters to discrete mechanical structures within the cell.

METHODS

Interferometer. The measurement of the microspheres was performed on the Veeco interference microscope NT 1100 with a green diode (center wavelength 535 m) used for illumination and 20× 0.28 NA Michelson through transmissive media (TTM) interference objective.[23] The NT 1100 in principle is an optical microscope with a Michelson interference objective that allows for the observation of not only lateral features with typical optical resolution (1.16 μm for the 20× objective) but also height dimensions below the scale of one nanometer.[24] The Michelson interferometer is composed of a beam splitter, reference mirror, and compensating fluid cell. The compensation cell is 0.7 mm thick bounded on both sides by 0.5 mm optical windows, thus matching the optical path length of a reflected beam from the test chamber. The CCD detector array is 640 × 480 pixels, which with a 20× objective produces a 315 × 240 μm field of view and a spatial sampling of 500 nm. The phase shifting interferometry (PSI) method was used to capture phase images of the cell bodies *in situ*. During measurement, a piezoelectric translator decreases the light path a small amount causing a phase shift between the test and reference beams. The system records the irradiance of the resulting interference pattern at many different phase shifts and then converts the irradiance to phase wavefront data by integrating the irradiance data using a PSI algorithm. The phase data are processed to remove phase ambiguities between adjacent pixels. Average optical thickness measurements for the regions of interest A1−A2 and B1−B2 were calculated by averaging the optical thickness across all pixels within the region, followed by subtracting the average thickness value from a similarly sized region adjacent to the cell containing no material. The external region served as a local reference for zero optical thickness. To determine the response to the cyclicly applied force (f = 0.05 Hz), the time varying data, sampled at 2 s intervals, was bandpass filtered around a center frequency f = 0.05 Hz.

Cell Chamber. The cell chamber body was constructed from machined nonmagnetic stainless steel. Resistive heating elements with internal thermistors, driven by a feedback controlled power supply, were used to regulate the chamber temperature to within 0.5 degrees of 37 °C. The fluid sample was contained within a 13 mm diameter, 0.7 mm thick sub chamber, having a 1 mm thick optical window on top and a 0.2 mm thick silicon floor.

Microspheres. Micrometer-sized elemental nickel microspheres were obtained from Duke Scientific as a dry powder. An aqueous suspension of microspheres was diluted 4:1 with 0.2% poly-L-lysine aqueous solution (Sigma) to inhibit aggregation and improve adhesion to the cell body. This microreflector solution was shaken vigorously before application to suspend any sedimented particles and reduce aggregates. A 200 μL portion of the suspension was pipetted onto the sample, and the microspheres were allowed to settle for 1 min.

Magnetic Force Control. Magnetic force was applied to the microspheres using a cylindrical rare earth magnet 7 mm in diameter by 21 mm long, oriented axially along the vertical direction below the test chamber. The magnet was positioned with a feedback controlled motorized micrometer, capable of <10 μm accuracy. The magnitude of magnetic flux perpendicular to the vertical axis, as a function of axial distance, was measured with a miniature Hall probe (2 mm × 2 mm) and a F.W. Bell 5180 gaussmeter accurate to 0.1 G. In the "off" position, the magnet was lowered to >4 cm below the sample, resulting in negligible field at the sample point. The magnet was positioned coaxially with the optical axis to ensure a uniform magnetic flux across the viewing area (~300 μm × 300 μm with the 20× objective). The force applied to the nickel microspheres as a function of magnet position was determined using microcantilever arrays tipped with elemental nickel or several uniformly magnetic microspheres (Compel 8 μm carboxylated microspheres, Bangs Laboratories). Each microcantilever is 500 μm long by 100 μm wide and 0.9 μm thick, with a nominal spring constant of 0.01 N/m. These commercially available arrays were produced by the IBM Zurich Research Laboratories using a proprietary dry etch, silicon-on-insulator (SOI) process. Using the optical profiler, the deflection of the reference cantilever could be determined to better that 1 nm. The volume magnetic moment for pure nickel (55 emu/g) was assumed for both the microspheres and the nickel film deposited on the cantilever tips. Pure nickel is completely magnetically polarized at field strengths of 200 G and higher, while the lowest field strength used in measurements was 500 G. Preceding measurements, the magnet was raised to with 1.5 mm of the sample, corresponding to a ~2 kG flux at the sample point, to ensure that the microspheres' magnetic moments were oriented axially.

In our experiment the range of applied forces are determined by the applied magnetic field and cover a range from 0 to 200 pN. Optical tweezers typically operate in the 100 fN to 100 pN range. AFM typically operates in the 100 pN and larger force range. In our case, we are applying ~200 pN of force on a 5 μm diameter bead. At small indentations (~500 nm) this amounts to less than 1 pN applied for per square nanometer. For comparison, the typical force generated by a single molecular motor is in the range of several pN, while the contractile force generated through the cytoskeleton of a whole cell may range from nN to mN. Antibody−antigen binding forces are on the order of nN.

Acknowledgment. This study was funded by NIH grant R21GM074509. Additional support was provided by the NIH Roadmap for Medical Research PN2EY018228, NIH grants R01CA90571, R01CA107300, R01GM073981. M.A.T. is a Scholar of the Leukemia and Lymphoma Society. The authors have no competing interest.

Supporting Information Available: Details of the magnetic field calibration and an extended discussion of the effects of microsphere size on cell dynamics and the *z*-axis resolution of LCI. This material is available free of charge *via* the Internet at http://pubs.acs.org.

REFERENCES AND NOTES

1. Kumar, S.; Maxwell, I. Z.; Heisterkamp, A.; Polte, T. R.; Lele, T. P.; Salanga, M.; Mazur, E.; Ingber, D. E. Viscoelastic Retraction of Single Living Stress Fibers and Its Impact on Cell Shape, Cytoskeletal Organization, and Extracellular Matrix Mechanics. *Biophys. J.* **2006**, *90*, 3762–3773.
2. Matthews, B. D.; Overby, D. R.; Mannix, R.; Ingber, D. E. Cellular Adaptation to Mechanical Stress: Role of Integrins, Rho, Cytoskeletal Tension and Mechanosensitive Ion Channels. *J. Cell Sci.* **2006**, *119*, 508–518.
3. Felsenfeld, D. P.; Schwartzberg, P. L.; Venegas, A.; Tse, R.; Sheetz, M. P. Selective Regulation of Integrin-Cytoskeleton Interactions by the Tyrosine Kinase Src. *Nat. Cell Biol.* **1999**, *1*, 200–206.
4. Lee, J.; Ishihara, A.; Oxford, G.; Johnson, B.; Jacobson, K. Regulation of Cell Movement Is Mediated by Stretch-Activated Calcium Channels. *Nature* **1999**, *400*, 382–386.
5. Yauch, R. L.; Felsenfeld, D. P.; Kraeft, S. K.; Chen, L. B.; Sheetz, M. P.; Hemler, M. E. Mutational Evidence for Control of Cell Adhesion through Integrin Diffusion/Clustering, Independent of Ligand Binding. *J. Exp. Med.* **1997**, *186*, 1347–1355.
6. Felsenfeld, D. P.; Choquet, D.; Sheetz, M. P. Ligand Binding Regulates the Directed Movement of Beta 1 Integrins on Fibroblasts. *Nature* **1996**, *383*, 438–440.
7. Chicurel, M. E.; Singer, R. H.; Meyer, C. J.; Ingber, D. E. Integrin Binding and Mechanical Tension Induce Movement of Mrna and Ribosomes to Focal Adhesions. *Nature* **1998**, *392*, 730–733.
8. Van Vliet, K.; Bao, G.; Suresh, S. The Biomechanics Toolbox: Experimental Approaches for Living Cells and Biomolecules. *Acta Mater.* **2003**, *51*, 5881–5905.
9. Creath, K., Schmit, J. Phase Shifting Interferometry. In *Encyclopedia of Modern Optics*; Guenther, B., Ed.; Elsevier Academic Press: Boston, MA, 2005; pp 364−374.
10. Bechinger, C.; Giebel, K. F.; Schnell, M.; Leiderer, P.; Deising, H. B.; Bastmeyer, M. Optical Measurements of Invasive Forces Exerted by Appressoria of a Plant Pathogenic Fungus. *Science* **1999**, *285*, 1896–1899.
11. Hayakawa, K.; Sato, N.; Obinata, T. Dynamic Reorientation of Cultured Cells and Stress Fibers under Mechanical Stress from Periodic Stretching. *Exp. Cell Res.* **2001**, *268*, 104–114.
12. Deng, L. H.; Fairbank, N. J.; Fabry, B.; Smith, P. G.; Maksym, G. N. Localized Mechanical Stress Induces Time-Dependent Actin Cytoskeletal Remodeling and Stiffening in Cultured Airway Smooth Muscle Cells. *Am. J. Physiol.-Cell Physiol.* **2004**, *287*, C440−C448.
13. Smith, P. G.; Deng, L. H.; Fredberg, J. J.; Maksym, G. N. Mechanical Strain Increases Cell Stiffness through Cytoskeletal Filament Reorganization. *Am. J. Physiol.-Lung Cell. Mol. Physiol.* **2003**, *285*, L456−L463.
14. Trepat, X.; Deng, L. H.; An, S. S.; Navajas, D.; Tschumperlin, D. J.; Gerthoffer, W. T.; Butler, J. P.; Fredberg, J. J. Universal Physical Responses to Stretch in the Living Cell. *Nature* **2007**, *447*, 592–U7.
15. Sheetz, M. P.; Sable, J. E.; Dobereiner, H. G. Continuous Membrane-Cytoskeleton Adhesion Requires Continuous Accommodation to Lipid and Cytoskeleton Dynamics. *Annu. Rev. Biophys. Biomol. Struct.* **2006**, *35*, 417–434.
16. Bausch, A. R.; Moller, W.; Sackmann, E. Measurement of Local Viscoelasticity and Forces in Living Cells by Magnetic Tweezers. *Biophys. J.* **1999**, *76*, 573–579.
17. Hu, S. H.; Chen, J. X.; Fabry, B.; Numaguchi, Y.; Gouldstone, A.; Ingber, D. E.; Fredberg, J. J.; Butler, J. P.; Wang, N. Intracellular Stress Tomography Reveals Stress Focusing and Structural Anisotropy in Cytoskeleton of Living Cells. *Am. J.Physiol.-Cell Physiol.* **2003**, *285*, C1082−C1090.
18. Bausch, A. R.; Ziemann, F.; Boulbitch, A. A.; Jacobson, K.; Sackmann, E. Local Measurements of Viscoelastic Parameters of Adherent Cell Surfaces by Magnetic Bead Microrheometry. *Biophys. J.* **1998**, *75*, 2038–2049.
19. Lim, C. T.; Zhou, E. H.; Quek, S. T. Mechanical Models for Living Cells - a Review. *J. Biomech.* **2006**, *39*, 195–216.
20. Stamenovic, D.; Fredberg, J. J.; Wang, N.; Butler, J. P.; Ingber, D. E. A Microstructural Approach to Cytoskeletal Mechanics Based on Tensegrity. *J. Theor. Biol.* **1996**, *181*, 125–136.
21. Wang, N.; Naruse, K.; Stamenovic, D.; Fredberg, J. J.; Mijailovich, S. M.; Toric-Norrelykke, I. M.; Polte, T.; Mannix, R.; Ingber, D. E. Mechanical Behavior in Living Cells Consistent with the Tensegrity Model. *Proc. Natl. Acad. Sci. U.S.A.* **2001**, *98*, 7765–7770.
22. Canadas, P.; Wendling-Mansuy, S.; Isabey, D. Frequency Response of a Viscoelastic Tensegrity Model: Structural Rearrangement Contribution to Cell Dynamics. *J. Biomech. Eng.-Trans. ASME* **2006**, *128*, 487–495.
23. Reed, J. W., P.; O Doherty, K.; Schmit, J.; Han, S.; Troke, J.; Teitell, M.; Klug, W.; Gimzewski, J. Applications of Imaging Interferometry. *Proc. SPIE -Int. Soc. Opt. Eng.* **2006**, *6293*, 629301.
24. Olszak, A. G.; Schmit, J.; Heaton, M. G. Interferometric Approaches Each Have Advantages. *Laser Focus World* **2001**, *37*, 93–95.